

# New Family of Ruthenium-Dye-Sensitized Nanocrystalline TiO<sub>2</sub> Solar Cells with a High Solar-Energy-Conversion Efficiency\*\*

By Kung-Shih Chen, Wei-Hsin Liu, Yu-Hsiu Wang, Chin-Hung Lai, Pi-Tai Chou,\* Gene-Hsiang Lee, Kellen Chen, Hsing-Yi Chen, Yun Chi,\* and Fu-Ching Tung

A new type of ruthenium complexes **6–8** with tridentate bipyridine–pyrazolate ancillary ligands has been synthesized in an attempt to elongate the  $\pi$ -conjugated system as well as to increase the optical extinction coefficient, possible dye uptake on TiO<sub>2</sub>, and photostability. Structural characterization, photophysical studies, and corresponding theoretical approaches have been made to ensure their fundamental basis. As for dye-sensitized solar cell applications, it was found that **6–8** possess a larger dye uptake of  $2.4 \times 10^{-7}$  mol cm<sup>-2</sup>,  $1.5 \times 10^{-7}$  mol cm<sup>-2</sup>, and  $1.3 \times 10^{-7}$  mol cm<sup>-2</sup>, respectively, on TiO<sub>2</sub> than that of the commercial N3 dye ( $1.1 \times 10^{-7}$  mol cm<sup>-2</sup>). Compound **8** works as a highly efficient photosensitizer for the dye-sensitized nanocrystalline TiO<sub>2</sub> solar cell, producing a 5.65 % solar-light-to-electricity conversion efficiency (compare with 6.01 % for N3 in this study), a short-circuit current density of 15.6 mA cm<sup>-2</sup>, an open-circuit photovoltage of 0.64 V, and a fill factor of 0.57 under standard AM1.5 irradiation (100 mW cm<sup>-2</sup>). These, in combination with its superior thermal and light-soaking stability, lead to the conclusion that the concomitant tridentate binding properties offered by the bipyridine–pyrazolate ligand render a more stable complexation, such that extended life spans of DSSCs may be expected.

## 1. Introduction

Owing to their versatility and low cost in view of their manufacturing,<sup>[1]</sup> dye-sensitized solar cells (DSSCs) have long been considered as a feasible alternative to conventional amorphous silicon solar cells. Typical DSSCs consist of a TiO<sub>2</sub> semiconductor electrode chemisorbed with sensitizers, a Pt-doped counter electrode, and an I<sup>-</sup>/I<sub>3</sub><sup>-</sup> redox mediator immersed in an electrolyte. The resulting devices have displayed not only high photoenergy conversion efficiency but also low fabrication costs, showing good prospect for future commercialization. For realizing these designs, many different dyes have been synthesized and tested. The most efficient sensitizers are *cis*-dithiocyanato bis(4,4'-dicarboxy-2,2'-bipyridine)ruthenium(II) and trithio-

cyanato-4,4',4''-tricarboxy-2,2':6',2''-terpyridine ruthenium(II) complexes, known as the N3 and black dye, respectively.<sup>[2]</sup> They are frequently employed in the fabrication of DSSCs due to their intense and wide-range absorption of visible light. They also have suitable ground- and excited-state energy levels with respect to the nanocrystalline TiO<sub>2</sub> conduction-band energy and they match the redox properties of the iodine/triiodide redox couple. However, these ruthenium(II) dyes still suffer from limitations especially in light-harvesting efficiency. Particularly, a higher response in the red and infrared spectral region and high dye uptake on TiO<sub>2</sub> are still demanded. Most attempts made to improve these shortcomings have unfortunately not all been significantly successful,<sup>[3]</sup> except for the case where two bithiophene fragments were incorporated into the dye and for which the reported incident-photon-to-current conversion efficiency (IPCE) is 10 % higher than that of its parent N3 dye under AM 1.5 simulated sunlight.<sup>[3f]</sup>

We report here a new design of organometallic sensitizers in an attempt to gain more understanding about the chemical and physical nature of the molecular functionality on solar-energy-conversion efficiency. To simplify the parameters, we have maintained the aforementioned bipyridine framework and at the same time have succeeded in fine-tuning the spectral properties of ruthenium polypyridyl complexes. To do this we have designed a novel tridentate bipyridine pyrazolate ligand, for which the preparation and chemistry are reminiscent to that of pyridyl pyrazolate ligands reported in the literature.<sup>[4]</sup> Our main focus lies in the possible extension of absorption in the far-visible region as well as an increase of the optical extinction coefficient. An increase in the uptake quantity of sensitizers is also required, such that dye-sensitized solar cells could be

[\*] Prof. P.-T. Chou, K.-S. Chen, W.-H. Liu, Y.-H. Wang, Dr. C.-H. Lai, G.-H. Lee

Department of Chemistry and Instrumentation Center  
National Taiwan University  
Taipei 106 (Taiwan)  
E-mail: chop@ntu.edu.tw

Prof. Y. Chi, K. Chen, H.-Y. Chen  
Department of Chemistry  
National Tsing Hua University  
Hsinchu 300 (Taiwan)  
E-mail: ychi@mx.nthu.edu.tw

F.-C. Tung  
Mechanical and Systems Research Laboratories  
Industrial Technology Research Institute  
Hsinchu 310 (Taiwan)

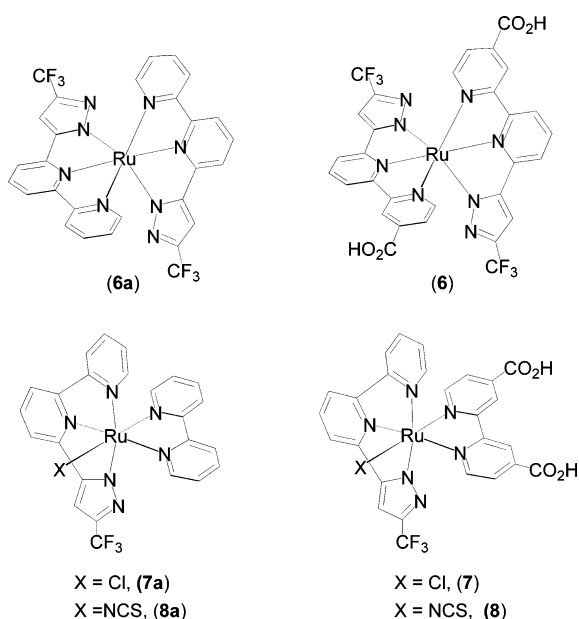
[\*\*] We thank the National Science Council, Taiwan for the financial support.

made thinner and thus more efficient because of reducing the transport losses in the nanoporous environment. Moreover, the strong  $\sigma$ -donor property of the pyrazolate unit, together with the good  $\pi$ -accepting ability of the second pyridyl fragment, provides a synergism of the electron delocalization over the whole ligand  $\pi$  conjugation as well as the metal  $d_{\pi}$  orbitals. As a result, the concomitant tridentate binding properties offered by the bipyridine pyrazolate ligand, thermodynamically, may render a more stable complexation than that of the terpyridine moiety on a similar ruthenium basis.<sup>[5]</sup> Thus, extending the life span of DSSCs may be expected. In this article, we report the strategic design, synthesis, and characterization of these newly designed ruthenium sensitizers as well as their potential application in DSSCs. These results should be complementary to those of the polyene-diphenylamine dye or other ruthenium(II)-based sensitizers, which were recently documented in the literature.<sup>[6]</sup>

## 2. Results

### 2.1. Strategic Design

As depicted in Scheme 1, in view of facile adsorption onto TiO<sub>2</sub>, we consider our target ruthenium sensitizers to be those possessing carboxyl function groups, namely compounds **6–8**.



**Scheme 1.** Structures of the ruthenium compounds.

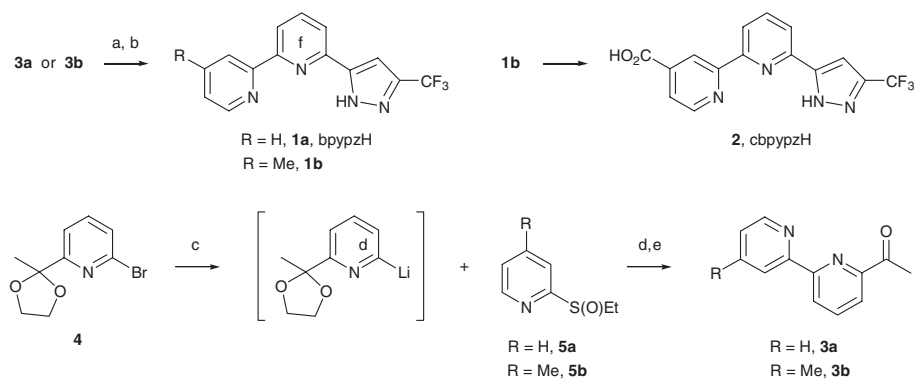
Three compounds are coordinated with at least one tridentate bipyridine pyrazolate chelate, which consists of the chelating bipyridine ligand linked to an anionic pyrazolate pendent. The introduction of the tridentate bipyridine pyrazolate chelate is expected to have certain advantages. First, the tridentate coordination mode makes the complex more stable against ligand dissociation on the coordination framework versus those com-

plexes possessing only monodentate and bidentate ligands or even terpyridine ligands (see above). Second, the extended  $\pi$ -conjugation over the tridentate ligand may induce a bathochromic shift of the ligand-centered bands as well as an increase in the molar extinction coefficients for the corresponding absorption signals; the latter is essential for showing high solar-absorption efficiency in the visible region. Moreover, the strong electron-donating nature of the negatively charged pyrazolate segment would destabilize the metal-centered  $d$ -orbital energy level, enhancing the participation of metal–ligand charge transfer (MLCT) transitions and possibly lowering the transition energy. Finally, the anionic nature of the pyrazolate fragment would allow it to be shared with the central ruthenium atom and/or the remaining auxiliary ligand in forming the highest occupied molecular orbital (HOMO) frontier orbital. The pyrazolate fragment, which is also pointed away from the TiO<sub>2</sub> surface, may act in a similar way to the thiocyanate ligand<sup>[7]</sup> and may facilitate the redox reaction with iodide in the surrounding electrolyte, promoting a faster electron transfer to the photoexcited metal complex.

Complex **8** possesses one typical 4,4'-dicarboxy-2,2'-bipyridine ligand, together with a tridentate bipyridine pyrazolate chelate and one thiocyanate (NCS) as the ancillary ligand. As a counterpart, complex **7** was synthesized, in which the NCS ligand was replaced by a chlorine atom, to examine the effect of NCS in this system regarding the performance of the DSSC. To extend the versatility, the homoleptic complex **6** was designed to investigate symmetry restriction which may significantly alter the photophysical properties, such as, absorption features, photostability, etc. Also, in comparison to compounds **7** and **8**, a substantial difference in physical properties, especially the adsorption cross section on TiO<sub>2</sub>, is expected for **6** because of its dual carboxylic groups attached at each terminal pyridine site of the tridentate bipyridine-pyrazolate chelate. Note that similar to complex **7**, no auxiliary ligand, such as, NCS, was introduced in complex **6**. We unfortunately failed to grow single-crystal complexes for **6–8**, possibly because of the attachment of carboxylic groups that inhibited crystal formation. Alternatively, single crystals of analogues of **6** and **8**, namely, **6a** and **8a**, in the absence of carboxylic groups, have been successfully prepared, such that valuable structural information can be extracted to mimic the structures of **6–8**.

### 2.2. Preparation of Tridentate Ligands

As depicted in Scheme 2, synthesis of the tridentate ligands **1a**, **1b**, and **2** required the prior preparation of 6-acetyl-2,2'-bipyridine derivatives (**3a**) and (**3b**) as the intermediates. These intermediates were prepared by the lithiation of 6-bromo-2-(2'-methyl-1',3'-dioxolan-2'-yl) pyridine (**4**), followed by nucleophilic addition of the lithio compound to ethyl 2-pyridyl sulfoxide compounds (**5a**) and (**5b**) according to the method documented in the literature.<sup>[8]</sup> Finally, acidic hydrolysis afforded the anticipated bipyridine derivatives **3a** and **3b** in good yield (see Scheme 2). Furthermore, compound **4** was obtained by treatment of 2-acetyl-6-bromopyridine with ethylene glycol in the presence of a catalytic amount of *p*-toluenesulfuric acid.



**Scheme 2.** Synthesis of tridentate ligands. a) CF<sub>3</sub>CO<sub>2</sub>Et, NaOEt, THF, reflux; b) N<sub>2</sub>H<sub>4</sub>, EtOH, reflux; c) *n*-BuLi, Et<sub>2</sub>O, -78 °C; d) THF, 25 °C; e) 2 M HCl, 60 °C, 2 h; f) K<sub>2</sub>Cr<sub>2</sub>O<sub>7</sub>/H<sub>2</sub>SO<sub>4</sub>.

The sulfoxide **5a** was obtained via a two-step protocol, involving a prior treatment of 2-mercaptopyridine with ethyl iodide to produce 2-(ethylmercapto)pyridine, followed by addition of magnesium monoperoxyphthalate. Accordingly, its 4-methyl substituted sulfoxide derivative **5b** was best prepared by selective lithiation of 4-picoline in the presence of 2-(dimethylamino)ethanol at 0 °C. This was followed by treatment with diethyl disulfide at -78 °C to afford 4-methyl-2-(ethylmercapto)pyridine<sup>[9]</sup> and, finally, sulfide-to-sulfoxide conversion using the same procedure involving magnesium monoperoxyphthalate reagent.

After this, the bipyridine-substituted pyrazole derivatives **1a** and **1b** were prepared by a Claisen condensation employing compounds **3a** (or **3b**) and ethyl trifluoroacetate, followed by treatment of the resulting  $\beta$ -diketone compounds with an excess of hydrazine monohydrate in refluxing ethanol. The <sup>1</sup>H-NMR spectra of **1a** and **1b** reflect their inherent low molecular symmetry. This is indicated by distinctive signals for all of the proton signals on both terminal and internal pyridyl fragments, while the unique N-H signal of pyrazole in CDCl<sub>3</sub> solvent appeared as a broad band centered at approx.  $\delta$  12.0 and 11.9, respectively. Finally, the carboxylic derivative **2** was obtained from dichromate oxidation of **1b** in a solution of conc. H<sub>2</sub>SO<sub>4</sub>.<sup>[10]</sup> The <sup>1</sup>H-NMR spectrum of **2** in d<sub>6</sub>-DMSO did agree with the proposed structure, showing seven aromatic protons in the region  $\delta$  = 9.17–7.48, while both of the carboxylate and pyrazolate protons were not detected under this condition.

### 2.3. Preparation of Ruthenium Complexes

The synthesis of the Ru<sup>II</sup> complexes **6a** and **6** was performed following standard procedures. Refluxing [RuCl<sub>2</sub>(DMSO)<sub>4</sub>] with two equiv. of ligand **1a** in ethanol gave, after chromatography on silica gel (ethyl acetate/acetone = 9:1), the corresponding complex **6a**, [Ru(bpyppz)<sub>2</sub>] (bpyppz: 5-(2,2'-bipyridin-6-yl)-3-(trifluoromethyl)-1H-pyrazole). The related carboxy-substituted derivative **6** was prepared in an analogous way using ligand **2**, followed by repeated recrystallization from hot acetone to purify the product. Both complexes were characterized by fast-atom-bombardment mass spectrometry (FABMS),

<sup>1</sup>H-NMR, and elemental analyses, the results of which were in accordance with the assigned structures. Single-crystal X-ray analysis on **6a** was conducted to confirm the proposed molecular structure.

The complex **6a** crystallized in the monoclinic space group C2/c with eight formula units per unit cell, showing the anticipated, mutually orthogonal meridional coordination mode for the tridentate bpyppz ligand (Fig. 1). The Ru-N(bpy) bond lengths range from 1.991 to 2.068 Å, compare with the average length for Ru-N = 2.056 Å in the cationic complex [Ru(bpy)<sub>3</sub>]<sup>2+</sup>,<sup>[11]</sup> whereas the Ru-N bond lengths of the

middle pyridyl substituents are notably shorter (1.991 Å). This can probably be attributed to the internal strain exerted by the chelate bonding.<sup>[12]</sup> Moreover, the Ru-N(pyrazolate) bond lengths span from 2.063–2.065 Å, which is in the range that has been observed in neutral ruthenium complexes, for instance, Ru-N<sub>(pz)</sub> = 2.046 Å in [Ru(ibpz)<sub>2</sub>(PPhMe<sub>2</sub>)<sub>2</sub>], where ibpz = 3-*tert*-butyl-5-(1-isoquinolyl) pyrazolate,<sup>[13]</sup> and 2.047 and 2.071 Å in [Ru(ibpz)<sub>2</sub>(dpp=)], where dpp = *cis*-1,2-bis-(diphenylphosphino)ethylene.<sup>[14]</sup> The N-Ru-N bite angle of the tridentate bpyppz ligands is also remarkable; that is, N(1)-Ru-N(3) = 157.0(1)° and N(5)-Ru-N(7) = 157.1(1)°. Despite of the presence of a slightly smaller pentagonal pyrazolate ring skeleton, which may give rise to larger chelating angles,

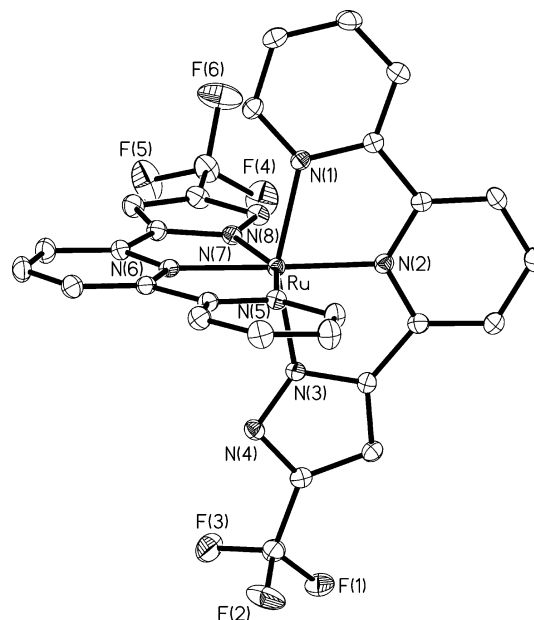


**Figure 1.** ORTEP diagram of **6a** with thermal ellipsoids shown at 30 % probability level; selective distances: Ru-N(1) = 2.065(2), Ru-N(2) = 1.991(3), Ru-N(3) = 2.063(2), Ru-N(5) = 2.068(2), Ru-N(6) = 1.991(3), Ru-N(7) = 2.065(2) Å and bond angles: N(1)-Ru-N(3) = 157.0(1), N(5)-Ru-N(7) = 157.1(1)°.

the detected bite angles are comparable to those of the various ruthenium terpyridine complexes, showing N–Ru–N angles of 157–159°. [15]

In an alternative approach to the required Ru<sup>II</sup> sensitizers, that is, **7** (**7a**) and **8** (**8a**), both bipyridine- and bipyridine-substituted pyrazole ligands were used together. This approach allowed not only the use of one highly conjugated, tridentate ligand to improve its absorption in the visible spectral region, but also the introduction of two carboxylic acid linkers on the bipyridine chelate, showing stronger bonding and good electronic communication to the TiO<sub>2</sub> surface. Complexes **8a** and **8** were synthesized using the multi-step protocol developed by Grätzel and co-workers. [16] It involves the prior treatment of bipyridine pyrazole bppyzH or cbppyzH with ruthenium reagent [RuCl<sub>2</sub>(*p*-cymene)<sub>2</sub>] in dimethylformamide (DMF) solution, followed by addition of bipyridine or 4,4'-dicarboxy-2,2'-bipyridine at higher temperatures to produce the chloride-substituted intermediate complexes **7a** and **7**, respectively. Finally, replacement of chloride with a thiocyanate ligand afforded the N-coordinated thiocyanate complexes **8a** and **8** in moderate yields.

Complex **8a** was also subjected to X-ray structural determination. As shown in Figure 2, its overall coordination geometry is best described as a distorted octahedron. It is noted that one bppyz ligand serves as a typical tridentate chelate with a significantly shorter Ru–N bond at the middle pyridyl fragment

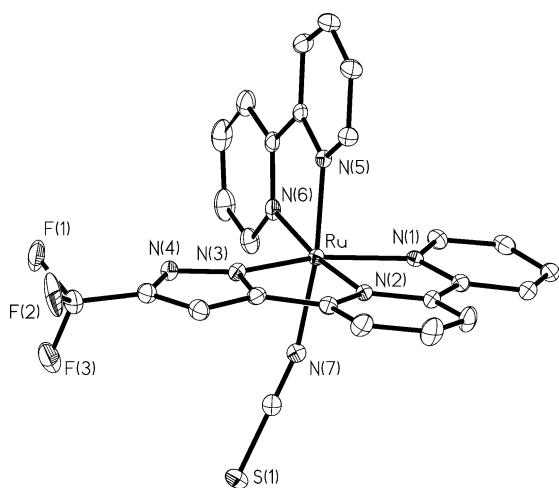


**Figure 2.** ORTEP diagram of **8a** with thermal ellipsoids drawn at 30% probability level; selective distances: Ru–N(1) = 2.069(4), Ru–N(2) = 1.972(4), Ru–N(3) = 2.049(4), Ru–N(5) = 2.036(4), Ru–N(6) = 2.060(4), Ru–N(7) = 2.053(4) Å and bond angles: N(1)–Ru–N(3) = 158.5(2), Ru–N(7)–C(25) = 163.1(4), N(7)–C(25)–S(1) = 178.4(4)°.

(Ru–N(2) = 1.972(4) Å) compared to the outer chelate bonding distances of Ru–N(1) = 2.069(4) and Ru–N(3) = 2.049(4) Å. The second bpy ligand adopts the unusual bidentate mode with slightly different bond distances Ru–N(5) = 2.036(4) and Ru–N(6) = 2.060(4) Å. The remaining sixth coordination site, which is located perpendicular to the tridentate ligand, is occupied by the N-coordinated thiocyanate with the Ru–N(7) dis-

tance being 2.053(4) Å. The bonding of thiocyanate ligand is reminiscent of that observed in [Ru(HP-terpy)(Me<sub>2</sub>-bpy)(NCS)], [17] for which the bent R–N–C angle and linear N–C–S arrangement are an indication of the efficient transfer of the Ru<sup>II</sup> d<sub>π</sub> electron density to the π-accepting thiocyanate ligand. [18] Finally, this gross coordination geometry around the Ru<sup>II</sup> metal atom is akin to that of the ionic complexes [Ru(tpy)(bpy)(H<sub>2</sub>O)]<sup>2+</sup> and [Os(tpy)(bpy)(H<sub>2</sub>O)]<sup>2+</sup> (tpy: 2,2',6',2''-terpyridine), [19] which showed the simultaneous coordination of tridentate and bidentate chelates as well as a monodentate ligand.

#### 2.4. Photophysical Characteristics and Device Properties

Figure 3 reveals the absorption spectra of **6**, **7**, and **8** in DMF. For comparison, the absorption spectrum of N3 is also depicted in Figure 3. With the same bipyridine chelate and NCS ligands, **8** and N3 show a similar absorption profile at the lowest transition (>550 nm), which can be tentatively ascribed to the MLCT in the singlet manifold (<sup>1</sup>MLCT). This transition incorporating bipyridine as a lowest unoccupied molecular orbital (LUMO) provider is ascertained by the similar absorption

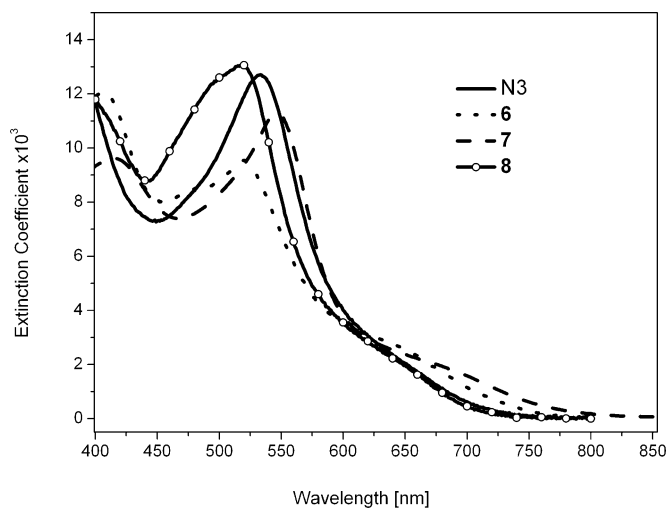


**Figure 3.** The absorption spectra in terms of the molar extinction coefficient for **6–8** and N3 in DMF solution.

extinction coefficient and the threshold wavelength of ca. 760 nm with respect to that of N3. Further support is given by the theoretical approach elaborated in the discussion section. The spectral range of 450–550 nm is tentatively assigned to the <sup>1</sup>π–π\* character mixed, in part, with <sup>1</sup>MLCT. In this region, the absorption extinction coefficient for **8** (520 nm, 13 056 M<sup>-1</sup> cm<sup>-1</sup>) is slightly higher than that of N3 (533 nm, 12 706 M<sup>-1</sup> cm<sup>-1</sup>), manifesting the contribution of the extending π-conjugation from the tridentate bipyridine pyrazolate ancillary ligands. Substituting NCS by Cl, forming **7**, results in a slight red shift of the spectral onset toward ca. 820 nm. This can be tentatively rationalized by the stronger π-electron donating Cl atom compared to NCS, causing a net effect of lifting

the d<sub>π</sub> electron and hence decreasing the lowest energy gap in **7**. Upon anchoring the carboxylic groups to each of the terminal pyridine of the tridentate bipyridine pyrazolate ligands, complex **6** exhibits a threshold wavelength at ca. 800 nm, the result of which, in comparison to **8**, may be rationalized by the extending π-electron delocalization throughout the tridentate bipyridine–pyrazolate, resulting in a decreased energy of the LUMO. In these cases, the lower lying transitions are expected to be manifested by a π–π\* transition mixed, in part, with MLCT in character. These viewpoints will be further verified via the theoretical approaches. Unfortunately, as shown in Figure 3, the associated molar extinction coefficient for both **6** and **7** is somewhat lower than that of **8** in the visible region.

Figure 4 depicts the absorption spectra of **6–8** and N3 adsorbed on an opaque TiO<sub>2</sub> film (15 μm thick). The solid-state absorption spectrum was obtained by an absorption spectrometer equipped with an integrating sphere (Jasco V-570 UV-vis spectrophotometer with integrating sphere attachment Model ISN-470) to prevent reflection loss. The absorbance (*A*) was

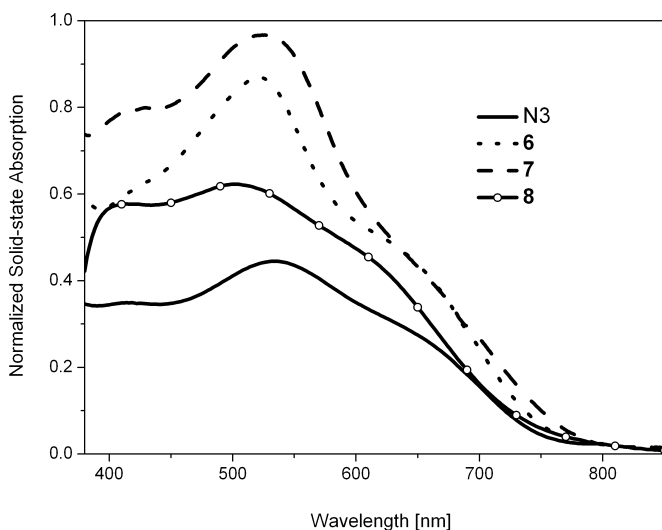


**Figure 4.** The absorption spectra of **6–8** and N3 adsorbed on TiO<sub>2</sub>. For clarity, the spectra were normalized at 800 nm.

calculated from the transmittance (*T* [%]) and reflectance (*R* [%]) by the following equation:

$$A = 1 - (T + R)\% \quad (1)$$

In comparison to the threshold wavelength of 820 and 760 nm in solution, the absorption spectra of **7** and **8** adsorbed on a TiO<sub>2</sub> film further shifts to ca. 850 and 800 nm, respectively. Similar to that reported for N3,<sup>[2a]</sup> the results may simply indicate a good electronic coupling between **8** (or **7**) and TiO<sub>2</sub>. Intriguingly, in comparison to **7** and **8**, negligible changes of the absorption profile compared to that in solution (DMF) were observed for **6** adsorbed on the TiO<sub>2</sub> film. This seems to imply that there is a weak electronic coupling between **6** and TiO<sub>2</sub>. It should be noted, however, that weak electronic coupling does

not necessarily imply low dye uptake on TiO<sub>2</sub>. The dye uptake of **6**, **7**, and **8** onto a TiO<sub>2</sub> film (15 μm thick) was determined to be 2.4 × 10<sup>-7</sup> mol cm<sup>-2</sup>, 1.5 × 10<sup>-7</sup> mol cm<sup>-2</sup>, and 1.3 × 10<sup>-7</sup> mol cm<sup>-2</sup>, respectively; these values are notably larger than that of the commercial N3 dye (1.1 × 10<sup>-7</sup> mol cm<sup>-2</sup>) conducted in this study. Moreover, despite its presumably weak electronic coupling with TiO<sub>2</sub>, **6** possesses the highest dye uptake and hence the highest coverage percentage; see Table 1.

We then fabricated DSSCs using the above complexes (see Experimental section for the detailed procedure). Prior to making the solar devices, cyclic voltammetry was performed to ensure that the LUMO of **6–8** were suited for injecting electrons into the conduction band of TiO<sub>2</sub>, and the electrochemical data of **6–8** are listed in Table 2. It is apparent that the redox potential of I<sup>-</sup>/I<sub>3</sub><sup>-</sup> (ca. 0.4 V versus the normal hydrogen electrode (NHE)) is more negative than the HOMO of **8** (or **6** and **7**) at 0.86 V (or 0.65 V and 0.54 V versus NHE) and is able to regenerate the dyes from electron donation. The lowest unoccupied molecular orbital (LUMO) of **8** (or **6** and **7**) at -1.02 V (or -1.16 V and -1.18 V versus NHE) is also energetically favorable to inject electrons into the conduction band of the TiO<sub>2</sub> electrode (-0.5 V versus NHE). Furthermore, the fabrication of DSSCs, composed of 0.25 cm<sup>2</sup> dye-adsorbed TiO<sub>2</sub> film and 0.05 M I<sub>2</sub>/0.1 M LiI, 0.5 M *t*-butylpyridine (tBPY)/0.6 M

**Table 1.** Calculations for dye molecule cross-sectional area and experimentally determined coverage percentage.

	Single molecular volume [a] [nm <sup>3</sup> ]	Cross-sectional area [b] [nm <sup>2</sup> ]	Dye Uptake [c] [mol/cm <sup>2</sup> ]	Coverage percentage [%]
N3	0.7753	1.020	1.1 × 10 <sup>-7</sup>	87%
<b>6</b>	0.7643	1.010	2.4 × 10 <sup>-7</sup>	184%
<b>7</b>	0.6059	0.866	1.5 × 10 <sup>-7</sup>	99%
<b>8</b>	0.7167	0.968	1.3 × 10 <sup>-7</sup>	96%

[a] Theoretical calculation results using a Hartree–Fock model can be used to derive molecular van der Waal radii, it is recommended, however, to add 0.5 Å when applied in solvent model calculations using Gaussian 03. [b] Estimated by assuming these dyes are ball-shaped with volume 4πr<sup>3</sup>/3. [c] Measured by a colorimetric method using NaOH solution to wash these dyes off the TiO<sub>2</sub> layer.

**Table 2.** Electrochemical data of ruthenium complexes **6–8** in DMF.

	E <sup>HOMO</sup> [a] [V] (vs. Fc/Fc <sup>+</sup> )	E <sup>LUMO</sup> [a] [V] (vs. Fc/Fc <sup>+</sup> )	E <sub>g</sub> [c] [V]	E <sub>g</sub> [d] [V]
<b>6</b>	0.35 (0.65) [b]	-1.16 (-0.86) [b]	1.51	1.61
<b>7</b>	0.24 (0.54) [b]	-1.18 (-0.88) [b]	1.42	1.51
<b>8</b>	0.56 (0.86) [b]	-1.02 (-0.72) [b]	1.58	1.66

[a] Values obtained with 1.0 × 10<sup>-3</sup> M solutions of complexes **6–8** in DMF using 0.10 M tetrabutylammonium tetrafluoroborate (TBABF<sub>4</sub>) as the supporting electrolyte. The redox potentials were calibrated using Fc/Fc<sup>+</sup>. [b] The values in the parentheses are the redox potentials versus NHE, which could be deduced from the equation: E<sup>HOMO/LUMO</sup> (vs. NHE) = E<sup>HOMO/LUMO</sup> (vs. Fc/Fc<sup>+</sup>) + 0.3 (Fc/Fc<sup>+</sup> redox potential vs. NHE). [c] Energy gap calculated from the difference of the HOMO and the LUMO energy level. [d] Energy gap calculated from the onset of the S<sub>1</sub> band of each complex.

butylmethylimidazolium iodide (BMII) in 1:1 methylcyanide (acetonitrile)/1-butyl cyanide (valeronitrile) solvent and 10% 3-methyl-2-oxazolidinone (NMO), was optimized for each complex, such that its maximum performance, at least in this study, was achieved under the optimized conditions. Figure 5 depicts the current–voltage curves for **6–8** and N3. Under standard AM 1.5 G irradiation, the maximum efficiency for the **8**-sensitized TiO<sub>2</sub> solar cell was calculated to be 5.65%, with a short-circuit current ( $J_{sc}$ ) of 15.6 mA cm<sup>-2</sup>, an open-circuit

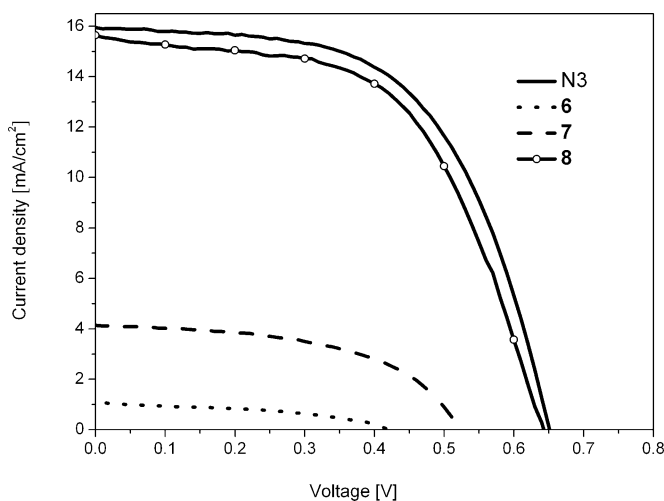


**Figure 5.** Photocurrent-density–voltage characteristics under AM 1.5 sunlight (100 mW cm<sup>-2</sup>) for N3, **6**, **7**, and **8**-based dye-sensitized solar cells.

photovoltage ( $V_{oc}$ ) of 0.64 V, and a fill factor (FF) of 0.57. To be able to make a fair comparison, the DSSC performance of N3 was also optimized in the current study. As a result, the efficiency for the N3-sensitized TiO<sub>2</sub> solar cell was 6.01%, with a  $J_{sc}$  of 15.9 mA cm<sup>-2</sup>, a  $V_{oc}$  of 0.65 V, and a fill factor (FF) of 0.58. In another approach, the conversion efficiency of the **6**-sensitized solar cell was apparently lower, with a  $J_{sc}$  of 1.11 mA cm<sup>-2</sup>, a  $V_{oc}$  of 0.42 V, a fill factor (FF) of 0.43, and consequently an energy-conversion efficiency of only 0.19% was deduced. The performance of the **7**-sensitized solar cell was in between that of **6** and **8**, with a  $J_{sc}$  of 4.13 mA cm<sup>-2</sup>, a  $V_{oc}$  of 0.52 V, and an energy-conversion efficiency of 1.14%.

Figure 6 shows the typical IPCE spectra obtained from nanocrystalline TiO<sub>2</sub> solar cells sensitized by compound **8** as well as N3 in this study. Visible light (400–800 nm) can be converted to a current with a maximum of 55% efficiency at 515 nm by the solar cell composed of **8**, producing a prominent photocurrent. Taking into account the light-absorption loss by fluorine-doped tin oxide (FTO)-coated glass, the IPCE of **8** and N3 is close to 60% from 500 to 650 nm (maximum 64% at 520 nm for **8** and 66% at 535 nm for N3). On the other hand, for **6** and **7**, the maximum IPCE was only 8% and 30%, respectively (not shown here). In comparison to that of complex **8**, the smaller  $\eta$  value found in **7** manifests the key role played by NCS in DSSCs. It has been proposed that the neces-

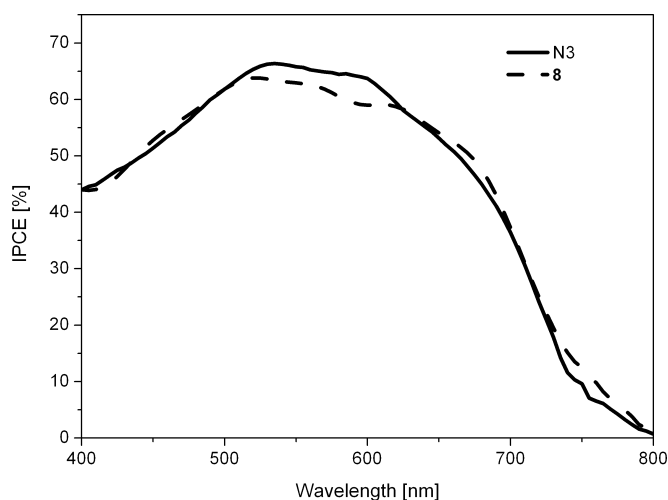


**Figure 6.** Incident-photon-to-electron efficiency (IPCE) of N3 and **8**-based dye-sensitized solar cell. Note that the loss-of-light source resulting from reflection of the FTO glass substrate has been taken into consideration.

sity of NCS lies in its contribution to the HOMO, such that, upon excitation, NCS acts as a hole acceptor that can subsequently contact with the outside redox couple, for instance,  $\Gamma/I_3^-$ , and fulfill the cycle on the reduction part. On the other hand, the much inferior performance for **6** can qualitatively be attributed to the low electronic coupling between **6** and the TiO<sub>2</sub> molecules in combination with possibly an improper orientation of the carboxylate group, see the discussion section. Finally, it is also worthy to note that for **6a**, **7a**, and **8a** that have a lack of carboxylic substituents, the current output for solar cells based on these compounds is < 0.1 mA, resulting in a negligible external quantum efficiency.

## 2.5. Thermal Properties and Light-Soaking Stability

Thermal and photostability were also key concerns in this study. For a comparative study between N3 and complex **8**, thermogravimetric analysis (TGA) measurements were carried out up to 800 °C. The decomposition temperatures of N3 and **8** were in the range of 330 to 400 °C, as shown in Figure 7, and the residue was considered to be char. The weight loss could be ascribed to ligand–dcby decomposition and was consistent with literature reports. The lower degree of weight loss in the lower temperature region for **8** versus that of N3 suggests that the replacement of one dcby ligand with the more stable tridentate ligand does effectively enhance its relative thermal stability.

As for the photostability, a complex **8**-sensitized cell was carefully sealed in a dry box and submitted to an aging test. Photocurrent versus voltage measurements were carried out at regular intervals, and the cell showed a good stability over a period of 500 h of light soaking at 55 °C. During the aging process, only a small fluctuation (< 5%) in efficiency was observed, supporting its high performance in view of DSSC applications.

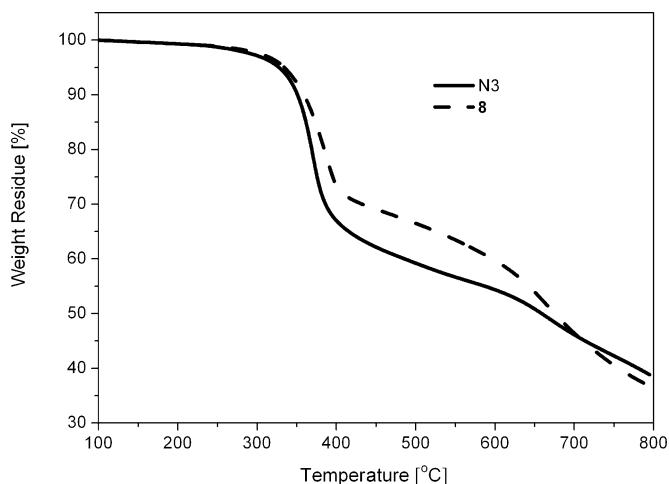


Figure 7. TGA results of N3 and **8** under N<sub>2</sub> atmosphere.

### 3. Discussion

In this section, we attempt to rationalize the above experimental results using a theoretical basis. To gain more insight into the differences in photophysical and hence perhaps DSSC properties among the complexes studied, theoretical approaches (time-dependent density functional theory (DFT), see Experimental) on corresponding molecular orbitals involved in the transition were carried out. For complexes **6–8**, the descriptions and the energy gap of each transition as well as the corresponding features of the unoccupied and occupied frontier orbitals mainly involved in the lower transitions are depicted in Figures 8–10, respectively. Among all complexes studied, the lowest transition in both singlet and triplet manifolds are in fact dominated by MLCT mixed with ligand  $\pi-\pi^*$  transition in

state	assignment	$E_{cal}$ [eV]	$\lambda_{cal}$ [nm]	$f$
<b>S</b> <sub>1</sub>	HOMO→LUMO (+97%)	1.81	684.2	0.0391
<b>T</b> <sub>1</sub>	HOMO→LUMO (+88%)	1.62	767.0	~0

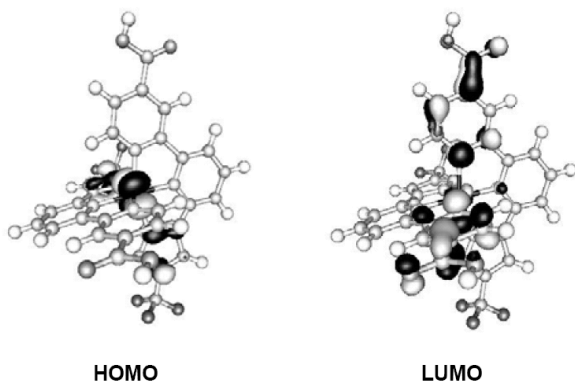


Figure 8. Theoretical calculations of the lower transition and the associated frontier orbitals of complex **6**.

state	assignment	$E_{cal}$ [eV]	$\lambda_{cal}$ [nm]	$f$
<b>S</b> <sub>1</sub>	HOMO→LUMO (+83%)	1.43	869.2	0.0184
<b>T</b> <sub>1</sub>	HOMO→LUMO (+100%)	1.16	1070	~0

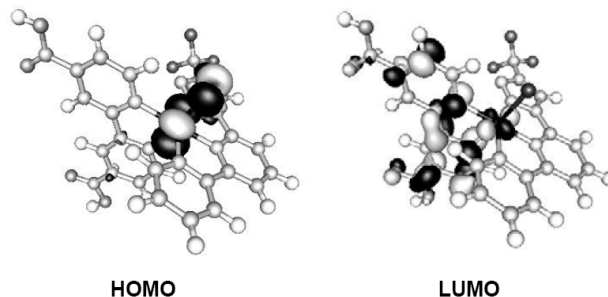


Figure 9. Theoretical calculations of the lower transition and the associated frontier orbitals of complex **7**.

state	assignment	$E_{cal}$ [eV]	$\lambda_{cal}$ [nm]	$f$
<b>S</b> <sub>1</sub>	HOMO→LUMO (+84%)	1.64	754.2	0.032
<b>T</b> <sub>1</sub>	HOMO→LUMO (+91%)	1.27	973.1	~0

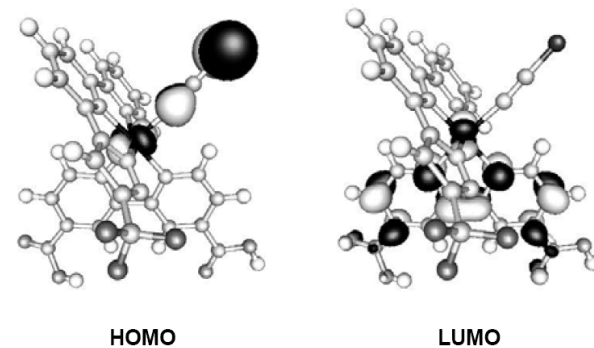


Figure 10. Theoretical calculations of the lower transition and the associated frontier orbitals of complex **8**.

character, in which the MLCT solely incorporates the Ru<sup>II</sup>  $d_{\pi} \rightarrow p$ -carboxylic pyridine transition. However, upon close examination, one can perceive a great difference between **6** and **8** (or **7**) as well as a subtle variation between **7** and **8** in view of the  $\pi-\pi^*$  (or  $n-\pi^*$ ) transition. For **6**, the  $\pi-\pi^*$  transition mainly originates from the pyrazolate to the terminal  $p$ -carboxylic pyridine, that is, an intraligand type of charge transfer (ILCT) within the tridentate pyridine pyrazolate. In sharp contrast, for both **7** and **8**, the  $\pi-\pi^*$  transition is ascribed as a ligand-to-ligand (interligand) type of charge transfer (LLCT) from the pyridine pyrazolate of the tridentate bipyridine pyrazolate to the  $p$ -dicarboxylic bipyridine. The ILCT in **6** can be viewed as a delocalization of the  $\pi$ -electron upon transition, rationalizing the lower energy gap observed experimentally. Moreover, comparing **7** and **8**, as expected, the density of the -NCS lone pair

electrons in **8** substantially contribute to the HOMO that is mainly involved in the lowest transition, that is, the  $n \rightarrow \pi^*$  transition. It should be noted that Grätzel and co-workers<sup>[20]</sup> have conducted INDO/S and DFT studies of the electronic and optical properties of their N3 derivative dye. The calculation pointed out that the top-three filled frontier orbitals are mainly composed of Ru 4d orbitals with a sizable contribution from the NCS ligand orbitals, whereas photoexcitation was directly charged into the carboxy bipyridine ligand bound to the TiO<sub>2</sub> surface. Our calculated results on complex **8** essentially follow a similar trend as that obtained by Grätzel and co-workers. Thus, in view of a similar light-to-electricity efficiency, independent of one thiocyanate group (**8**) or two (e.g., N3), the thiocyanate ligand can always couple with the Ru<sup>II</sup>  $d_{\pi}$  orbital, such that upon HOMO  $\rightarrow$  LUMO excitation, the hole carrier migrates to NCS and carries out the subsequent reduction in a very efficient manner. This explains well the superior DSSC performance of **8** over that of **7**. As listed in Figures 9 and 10, both  $S_0-S_1$  and  $S_0-T_1$  energy gaps were calculated to be lower in **7**, which is consistent with the experimental results as well as the empirical approach in that the chlorine atom (in **7**) is a stronger  $\pi$ -electron-donating group with a net result of pushing up the Ru<sup>II</sup>  $d_{\pi}$  electron and hence decreasing the energy gap. The fact that compound **6** had the worst performance can be explained as follows: one obvious obstacle surely lies in having just a single carboxy pendent on each chelating ligand, as opposed to the dual carboxylic groups on **8** (or **7**), which is supported by the much weaker coupling between **6** and TiO<sub>2</sub> observed experimentally. Furthermore, as depicted in Figure 8, in contrast to the resonant delocalization of the LUMO electrons between two carboxylic groups for the bipyridine in **7** and **8**, each carboxylic substituent acts as an individual part with negligible cross talk in **6**. Such a configuration drastically diminishes the efficiency of electron injecting into the bound TiO<sub>2</sub>, if there is any coupling, rationalizing the much inferior DSSC performance in **6**. Finally, as shown in Figures 8–10, the theoretically predicted absorption wavelength in either singlet and triplet manifold is largely red shifted in comparison to that of the experimental results. As for the origin of this deviation, in addition to having neglected the solvation effect in the calculation, other possible resources must be considered at the current stage. In this study, a nodeless relativistic effective potential was used, the method of which has raised skepticism because of its limited reliability.<sup>[21]</sup> Moreover, due the molecular complexity, the current applied method is limited to PBE0 and 6-31G\* basis sets, which may not be high enough to warrant the required precision. Nevertheless, the theoretical level adopted here is suitable for interpreting the trend of photophysical and device properties for the complexes concerned.

## 4. Conclusions

In summary, a new family of ruthenium complexes has been designed and synthesized, in which **8** successfully acts as an efficient photosensitizer for DSSCs, with light-to-electricity con-

version efficiencies ( $\eta$ ) up to 5.65 % (versus 6.01 % for N3 obtained in this study). Supplemented by spectroscopic data and theoretical approaches, in comparison to N3, the increase of absorptivity at 450–550 nm in **8** can be rationalized by the  $\pi$ -electron delocalization spread over the tridentate bipyridine pyrazolate ligand. The ILCT (**6**) versus LLCT (**8**) for the lowest transition causes a lower energy gap in **6**, emphasizing the importance of the elongation of  $\pi$ -conjugation in tuning the energy gap. Although a higher dye uptake and extended absorption tail in the lower energy region were found, negligible coupling interaction with TiO<sub>2</sub> for **6** and the lack of a hole-transport ligand (NCS) for **7** (**6** as well) are believed to be key factors to account for their inferior DSSC performance compared to that of **8**. Although the  $\eta$  value and IPCE performance of **8** are more or less equal to N3 under the current DSSC configuration, its higher dye uptake on TiO<sub>2</sub> may warrant future design of thinner cells and thus more conversion efficiency because of possibly reducing the transport losses in the nanoporous environment. This, in combination with its superior thermal and light-soaking stability (see above), leads us to conclude that the concomitant tridentate binding properties offered by the bipyridine–pyrazolate ligand may render a more stable complexation, such that extending the lifespan of DSSCs is expected.

## 5. Experimental

### 5.1. General Information and Materials

Elemental analyses and mass spectra (operating in either FAB or ESI modes) were carried out at the NSC Regional Instrument Centre at the National Chiao Tung University, Taiwan. <sup>1</sup>H- and <sup>13</sup>C-NMR spectra were recorded on a Varian Mercury 400 or an Inova-500 MHz instrument; chemical shifts were quoted with respect to the internal standard Me<sub>4</sub>Si. All synthetic manipulations were performed under N<sub>2</sub> atmosphere, while solvents were used as received. RuCl<sub>3</sub> hydrate was purchased from Precious Metals Online, Australia, while [Ru(DMSO)<sub>4</sub>Cl<sub>2</sub>] and [RuCl<sub>2</sub>(*p*-cymene)<sub>2</sub>] were prepared by heating of RuCl<sub>3</sub> hydrate in dimethylsulfoxide (DMSO) and with 2-methyl-5-(1-methylethyl)-1,3-cyclohexadiene (*a*-phellandrene) in ethanol according to previously published methods [22].

### 5.2. Preparations

**Preparation of 1a and 1b.** To a stirred mixture of NaOEt (1.04 g, 15.6 mmol) and THF (50 mL) at 0 °C was added a 20 mL solution of 6-acetyl-2,2'-bipyridine (**3a**, 2.0 g, 10.1 mmol) in THF, followed by addition of ethyl trifluoroacetate (1.5 mL, 11.4 mmol). The mixture was refluxed for 12 h and the reaction was quenched with 2 M HCl until pH 8–9. Then the mixture was extracted with ethyl acetate (2 × 100 mL) and combined. The extracts were then washed with deionized water, dried over anhydrous MgSO<sub>4</sub>, and concentrated in vacuum to give the diketone (2.7 g).

Without further purification, the hydrazine monohydrate (98 %, 4.2 mL, 86.0 mmol) was added into a solution of diketone reagent in EtOH (60 mL). After heating under reflux for 12 h, the solvent was removed under vacuum. The residue was dissolved in CH<sub>2</sub>Cl<sub>2</sub> (100 mL), and the solution was washed with water, dried over anhydrous MgSO<sub>4</sub>, and concentrated. Finally, the product was purified by silica-gel column chromatography using a 1:1 mixture of hexane and ethyl acetate, giving **1a** as colorless solid (1.2 g, 40 %). The methyl derivative **1b** was prepared using similar procedures.

Spectral data of **1a**: <sup>1</sup>H-NMR (400 MHz, d<sub>6</sub>-DMSO): δ [ppm]: 8.88 (d, *J*<sub>HH</sub> = 8.0 Hz, 1H), 8.69 (d, *J*<sub>HH</sub> = 4.8 Hz, 1H), 8.39 (d, *J*<sub>HH</sub> = 7.6 Hz, 1H), 8.06 (t, *J*<sub>HH</sub> = 7.6 Hz, 1H), 8.01–7.97 (m, 2H), 7.49–7.46 (m, 2H).

Spectral data of **1b**: MS (EI): *m/z* 304 (M<sup>+</sup>). <sup>1</sup>H-NMR (400 MHz, d<sub>6</sub>-DMSO): δ [ppm]: 8.76 (s, 1H), 8.54 (d, *J*<sub>HH</sub> = 4.8 Hz, 1H), 8.38 (d, *J*<sub>HH</sub> = 8.0 Hz, 1H), 8.06 (t, *J*<sub>HH</sub> = 7.6 Hz, 1H), 7.99 (d, *J*<sub>HH</sub> = 7.6 Hz, 1H), 7.53 (s, 1H), 7.32 (d, *J*<sub>HH</sub> = 4.8 Hz, 1H), 2.47 (s, 3H).

**Preparation of 2.** A solid sample of **1b** (0.7 g, 2.30 mmol) was slowly added to a vigorously stirred solution of sulfuric acid (98%, 16 mL). Next, 1.6 g of K<sub>2</sub>Cr<sub>2</sub>O<sub>7</sub> was added in small portions, keeping the temperature below 80 °C. The mixture was stirred until the temperature gradually decreased back to RT. The deep green mixture was poured into 100 mL of ice-water mixture, and left overnight at 5 °C. The precipitate was filtered and washed with water. This solid was transferred into 16 mL of 1:1 water and 98% nitric acid and refluxed for 5 h. The solution was allowed to cool to RT and was poured into 200 mL of ice water and kept at 5 °C overnight. The precipitate was filtered, washed with water (2 × 10 mL) and Et<sub>2</sub>O (2 × 5 mL), giving 0.51 g of a colorless solid **2** (cbppyzH, 67%), cbppyzH: 5-(4'-carboxy-2,2'-bipyridin-6-yl)-3-(trifluoromethyl)-1H-3-pyrazole.

Spectral data of **2**: MS (EI): *m/z* 334 (M<sup>+</sup>). <sup>1</sup>H-NMR (400 MHz, d<sub>6</sub>-DMSO): δ [ppm]: 9.17 (s, 1H), 8.89 (d, *J*<sub>HH</sub> = 4.8 Hz, 1H), 8.44 (d, *J*<sub>HH</sub> = 7.6 Hz, 1H), 8.11 (t, *J*<sub>HH</sub> = 8.0 Hz, 1H), 8.03 (d, *J*<sub>HH</sub> = 8.0 Hz, 1H), 7.90 (d, *J*<sub>HH</sub> = 4.8 Hz, 1H), 7.48 (s, 1H).

**Preparation of 6.** A solution of **2** (50 mg, 0.15 mmol) and Ru(DMSO)<sub>4</sub>Cl<sub>2</sub> (36 mg, 0.074 mmol) in ethanol (20 mL) was heated under reflux for 12 hr. After cooling the solution to RT, the solvent was removed and the residue was recrystallized from hot acetone (3 × 5 mL), giving analytical pure [Ru(cbppyz)<sub>2</sub>] as a dark brown solid (**6**, 21 mg, 40%).

Spectral data of **6**: MS (FAB, <sup>102</sup>Ru): *m/z* 768 (M<sup>+</sup>). <sup>1</sup>H-NMR (400 MHz, CD<sub>3</sub>OD, 298 K): δ [ppm]: 8.94 (s, 1H), 8.78 (d, 1H, *J*<sub>HH</sub> = 8.0 Hz), 8.52 (d, 1H, *J*<sub>HH</sub> = 8.0 Hz), 8.36 (t, 1H, *J*<sub>HH</sub> = 8.0 Hz), 7.65 (d, 1H, *J*<sub>HH</sub> = 6.0 Hz), 7.62 (s, 1H), 7.49 (d, 1H, *J*<sub>HH</sub> = 5.2 Hz). Anal. Calcd. for C<sub>30</sub>H<sub>16</sub>F<sub>6</sub>N<sub>8</sub>O<sub>4</sub>Ru·6H<sub>2</sub>O: C, 40.32; H, 3.38; N, 12.54. Found: C, 40.42; H, 3.19; N, 12.32. The resulting analytical sample may contain 6 equivalents of water solvates.

**Preparation of 6a.** A solution of **1a** (100 mg, 0.35 mmol) and Ru(DMSO)<sub>4</sub>Cl<sub>2</sub> (80 mg, 0.17 mmol) in anhydrous ethanol (25 mL) was heated under reflux for 12 hr. After cooling the solution to RT, the solvent was removed and the residue was subjected to silica-gel column chromatography (ethyl acetate/acetone = 9:1), giving [Ru(bpypz)<sub>2</sub>] as a dark brown solid (**6a**, 50 mg, 43%). Crystals suitable for X-ray diffraction study were obtained from a slow diffusion of diethyl ether into a saturated methanol solution at RT.

Spectral data of **6a**: MS (FAB, <sup>102</sup>Ru): *m/z* 680 (M<sup>+</sup>). <sup>1</sup>H-NMR (400 MHz, CD<sub>3</sub>OD, 298 K): δ [ppm]: 8.38 (d, 1H, *J*<sub>HH</sub> = 4 Hz), 8.36 (d, 1H, *J*<sub>HH</sub> = 4.0 Hz), 8.13 (d, 1H, *J*<sub>HH</sub> = 8.0 Hz), 8.04 (t, 1H, *J*<sub>HH</sub> = 8.0 Hz), 7.69 (td, 1H, *J*<sub>HH</sub> = 8.0 and 2.0 Hz), 7.19 (d, 1H, *J*<sub>HH</sub> = 5.0 Hz), 7.09 (s, 1H), 7.02 (td, 1H, *J*<sub>HH</sub> = 6.6 and 1.2 Hz). Anal. Calcd. for C<sub>28</sub>H<sub>16</sub>N<sub>8</sub>F<sub>6</sub>Ru: N, 16.49; C, 49.49; H, 2.37. Found: N, 15.89; C, 49.04; H, 2.74.

Crystal data for **6a**: C<sub>31.5</sub>H<sub>32</sub>F<sub>6</sub>N<sub>8</sub>O<sub>4.5</sub>Ru, *M* = 809.72, monoclinic, space group *C2/c*, *T* = 150 K, *a* = 32.2734(3) Å, *b* = 15.4469(1) Å, *c* = 14.0513(1) Å, β = 104.4789(6), *U* = 6782.43(9) Å<sup>3</sup>, *Z* = 8, λ (MoKα) = 0.7107 Å, μ = 0.547 mm<sup>-1</sup>, 45 334 reflections collected, 7783 unique (*R*<sub>int</sub> = 0.0470), goodness-of-fit (GOF) = 1.076, final *wR*<sub>2</sub>(all data) = 0.1320. *R*<sub>1</sub>[*I* > 2σ(*I*)] = 0.0424.

**Preparation of 7.** In a typical synthesis, bpypzH (190 mg, 0.66 mmol) and [RuCl<sub>2</sub>(*p*-cymene)<sub>2</sub>] (200 mg, 0.33 mmol) were dissolved in a DMF solution (15 mL). The reaction mixture was heated to 60 °C for 4 h under constant stirring. After that, 4,4'-dicarboxy-2,2'-bipyridine (H<sub>2</sub>-dcbpy) (160 mg, 0.66 mmol) was added and the mixture was heated to 150 °C for another 4 h. After cooling the mixture to RT, the solvent was removed under vacuum. The resulting dark brown residue was suspended in a mixture of DMF (ca. 2 mL) and acetonitrile (7 mL) and then sonicated for 20 min. Finally, the precipitate was col-

lected by centrifugation and washing with acetonitrile and diethyl ether in sequence, giving a dark brown solid [Ru(bpypz)(H<sub>2</sub>-dcbpy)Cl] (**7**, 200 mg, 46%).

Spectral data of **7**: MS (ESI, <sup>102</sup>Ru): *m/z* 670 (M<sup>+</sup>). <sup>1</sup>H-NMR (400 MHz, d<sub>6</sub>-DMSO): δ [ppm]: 10.33 (d, *J*<sub>HH</sub> = 5.6 Hz, 1H), 9.10 (s, 1H), 8.83 (s, 1H), 8.56 (d, *J*<sub>HH</sub> = 8.4 Hz, 1H), 8.43 (d, *J*<sub>HH</sub> = 7.6 Hz, 1H), 8.29 (d, *J*<sub>HH</sub> = 5.6 Hz, 1H), 8.09 (d, *J*<sub>HH</sub> = 8.0 Hz, 1H), 8.03 (t, *J*<sub>HH</sub> = 7.6 Hz, 1H), 7.87 (t, *J*<sub>HH</sub> = 6.0 Hz, 1H), 7.55 (d, *J*<sub>HH</sub> = 6.4 Hz, 1H), 7.46 (d, *J*<sub>HH</sub> = 6.0 Hz, 1H), 7.43 (d, *J*<sub>HH</sub> = 6.0 Hz, 1H), 7.21 (m, 2H). Anal. Calcd. for C<sub>26</sub>H<sub>16</sub>ClF<sub>3</sub>N<sub>6</sub>O<sub>4</sub>Ru·1.5 DMF: C, 46.95; H, 3.40; N, 13.47. Found: C, 47.22 H, 3.20; N, 13.29. This analytical data showed the possible incorporation of 1.5 DMF solvate molecules.

**Preparation of 7a.** The procedures were identical to that of **7** but using bpypzH (610 mg, 2.10 mmol), [RuCl<sub>2</sub>(*p*-cymene)<sub>2</sub>] (600 mg, 0.99 mmol), and 2,2'-bipyridine (330 mg, 2.1 mmol) as the starting materials. After the removal of solvent, purification by silica-gel column chromatography (ethyl acetate/acetone = 1:1) gave a dark brown solid [Ru(bpypz)(bpy)Cl] (**7a**, 843 mg) in 69% yield.

Spectral data of **7a**: MS (FAB, <sup>102</sup>Ru): *m/z* 582 (M<sup>+</sup>). <sup>1</sup>H-NMR (400 MHz, d<sub>6</sub>-DMSO, 298 K): δ [ppm]: 10.14 (d, 1H, *J*<sub>HH</sub> = 8.0 Hz), 8.72 (d, 1H, *J*<sub>HH</sub> = 8.0 Hz), 8.47 (dd, 2H, *J*<sub>HH</sub> = 12.0 and 8.0 Hz), 8.35 (d, 1H, *J*<sub>HH</sub> = 8.0 Hz), 8.15 (d, 1H, *J*<sub>HH</sub> = 8.0 Hz), 8.02 (d, 1H, *J*<sub>HH</sub> = 8.0 Hz), 7.94–7.88 (m, 2H), 7.79 (t, 1H, *J*<sub>HH</sub> = 8.0 Hz), 7.59 (t, 1H, *J*<sub>HH</sub> = 8.0 Hz), 7.22 (t, 2H, *J*<sub>HH</sub> = 8.0 Hz), 7.16 (s, 1H), 7.00 (t, 1H, *J*<sub>HH</sub> = 8.0 Hz). Anal. Calcd. for C<sub>24</sub>H<sub>16</sub>ClF<sub>3</sub>N<sub>6</sub>Ru·1H<sub>2</sub>O: C, 48.05; H, 3.02; N, 14.01. Found: C, 47.87; H, 3.40; N, 13.41. This analytical data showed the association of one water solvate.

**Preparation of 8.** A mixture of [Ru(bpypz)(H<sub>2</sub>-dcbpy)Cl] (100 mg, 0.15 mmol) and NH<sub>4</sub>NCS (340 mg, 4.5 mmol) in 15 mL of DMF was heated to 140 °C for 5 h under constant stirring. After cooling the mixture to room temperature, the volatile was removed under vacuum and the residue was suspended in deionized water (10 mL) and sonicated for 10 min. The precipitated solid was collected by centrifugation followed by washing with acetonitrile and diethyl ether. Finally, the dark brown thiocyanate complex [Ru(bpypz)(H<sub>2</sub>-dcbpy)NCS] (**8**) was dried under vacuum, yield: 80 mg, 77%.

Spectral data of **8**: MS (ESI, <sup>102</sup>Ru): *m/z* 693 (M<sup>+</sup>). <sup>1</sup>H-NMR (400 MHz, d<sub>6</sub>-DMSO): δ [ppm]: 9.74 (d, *J*<sub>HH</sub> = 6.0 Hz, 1H), 9.16 (s, 1H), 8.91 (s, 1H), 8.63 (d, *J*<sub>HH</sub> = 8.0 Hz, 1H), 8.51 (d, *J*<sub>HH</sub> = 7.6 Hz, 1H), 8.37 (d, *J*<sub>HH</sub> = 5.6 Hz, 1H), 8.16 (m, 2H), 7.96 (t, *J*<sub>HH</sub> = 8.0 Hz, 1H), 7.60 (d, *J*<sub>HH</sub> = 4.8 Hz, 1H), 7.51 (m, 2H), 7.29 (m, 2H). Anal. Calcd. for C<sub>27</sub>H<sub>16</sub>F<sub>3</sub>N<sub>7</sub>O<sub>4</sub>RuS·1H<sub>2</sub>O: C, 45.64; H, 2.55; N, 13.80. Found: C, 45.42; H, 2.88; N, 13.80. This analytical sample showed the association of one water solvate.

**Preparation of 8a.** Similar to the procedures reported for **8**, treatment of [Ru(bpypz)(bpy)Cl] (**7a**, 120 mg, 0.21 mmol) with NH<sub>4</sub>NCS (150 mg, 2.1 mmol) in 25 mL of DMF gave a dark-brown thiocyanate complex [Ru(bpypz)(bpy)NCS] (**8a**, 99 mg, 0.16 mmol) in 80% yield. Single crystals of **8a** suitable for X-ray diffraction study were obtained by a slow diffusion of diethyl ether into the saturated methanol solution at RT.

Spectral data of **8a**: MS (FAB, <sup>102</sup>Ru): *m/z* 605 (M<sup>+</sup>). <sup>1</sup>H-NMR (400 MHz, d<sub>6</sub>-DMSO, 298 K): δ [ppm]: 9.56 (d, 1H, *J*<sub>HH</sub> = 6.0 Hz), 8.80 (d, 1H, *J*<sub>HH</sub> = 8.0 Hz), 8.59 (d, 1H, *J*<sub>HH</sub> = 8.0 Hz), 8.54 (d, 1H, *J*<sub>HH</sub> = 8.0 Hz), 8.45 (d, 1H, *J*<sub>HH</sub> = 8.0 Hz), 8.23 (t, 1H, *J*<sub>HH</sub> = 8.0 Hz), 8.02 (d, 1H, *J*<sub>HH</sub> = 8.0 Hz), 8.12–8.04 (m, 2H), 8.00 (t, 1H, *J*<sub>HH</sub> = 6.0 Hz), 7.94–7.90 (m, 2H), 7.72 (t, 1H, *J*<sub>HH</sub> = 8.0 Hz), 7.58 (d, 1H, *J*<sub>HH</sub> = 6.0 Hz), 7.31 (t, 1H, *J*<sub>HH</sub> = 6.0 Hz), 7.24 (s, 1H), 7.19 (d, 1H, *J*<sub>HH</sub> = 4.0 Hz), 7.09 (t, 1H, *J*<sub>HH</sub> = 6.0 Hz). Anal. Calcd. for C<sub>25</sub>H<sub>16</sub>F<sub>3</sub>N<sub>7</sub>RuS·1H<sub>2</sub>O: C, 48.90; H, 3.47; N, 15.35. Found: C, 49.06; H, 3.20; N, 15.29. This analytical sample showed the association of one water solvate.

Crystal data for **8a**: C<sub>25</sub>H<sub>16</sub>F<sub>3</sub>N<sub>7</sub>RuS, *M* = 604.58, orthorhombic, space group *Pbcn*, *T* = 150 K, *a* = 21.9073(8) Å, *b* = 14.5021(5) Å, *c* = 16.8249(6) Å, *U* = 5345.3(3) Å<sup>3</sup>, *Z* = 8, λ (MoKα) = 0.7107 Å, μ = 0.713 mm<sup>-1</sup>, 33 271 reflections collected, 6136 unique (*R*<sub>int</sub> = 0.0494), GOF = 1.187, final *wR*<sub>2</sub>(all data) = 0.1924. *R*<sub>1</sub>[*I* > 2σ(*I*)] = 0.0587.

### 5.3. X-ray Diffraction Studies

Single crystal X-ray diffraction data were measured on a Bruker SMART Apex CCD diffractometer using (Mo K $\alpha$ ) radiation ( $\lambda = 0.71073$  Å). The data collection was executed using the SMART program. Cell refinement and data reduction were performed with the SAINT program. The structure was determined using the SHELXTL/PC program and refined using full-matrix least squares. It was observed that single crystals of **6a** and **8a** possessed two DMSO molecules and 3.5 methanol plus one water hydrate in the unit cell, respectively. Their crystallographic data (excluding structure factors) have been deposited at the Cambridge Crystallographic Data Centre with the deposition numbers 624672 and 624673, respectively. These data can be obtained free of charge by applying to the CCDC, 12 Union Road, Cambridge CB21EZ, UK (fax: (+44) 1223-336-033; E-mail: deposit@ccdc.cam.ac.uk)

### 5.4. Fabrication of DSSC

TiO<sub>2</sub> nanoparticles were purchased in a 25% rutile and 75% anatase mixture from Degussa. TiO<sub>2</sub> thin films were prepared by a doctor-blade method on a transparent conducting oxide (F-doped SnO<sub>2</sub>, FTO) and then sintered at 450 °C for 30 min. Nanocrystalline TiO<sub>2</sub> films (14–15  $\mu\text{m}$  thick) were coated with dyes by dipping the film in  $3 \times 10^{-4}$  M dye solutions in DMF overnight. The dye-coated TiO<sub>2</sub> electrode was incorporated into a thin-layer sandwich-type cell with a Pt-coated FTO as counter electrode, a spacer film, and an organic electrolyte solution to measure the solar cell performance. The Pt counter-electrode was prepared by spin-coating a 5 mM H<sub>2</sub>PtCl<sub>6</sub> in isopropyl alcohol solution on FTO glass followed by sintering at 385 °C for 15–30 min [23]. The electrolyte contained 0.05 M I<sub>2</sub>, 0.1 M LiI, 0.5 M *t*-butylpyridine (tBPY), and 0.6 M butylmethylimidazolium iodide (BMII) in 1:1 acetonitrile/valeronitrile solvent and 10% 3-methyl-2-oxazolidinone (NMO) was used (in volume ratio) [24]. Light-to-electricity conversion efficiency values were measured using a standard AM 1.5 solar simulator-Oriel 66924 Arc lamp source with a 6266 450 W Xe lamp, and Oriel 81088 Air Mass 1.5 Global Filter and a digital source meter which was purchased from the Keithley company.

### 5.5. Adsorption Cross Section on TiO<sub>2</sub>

In this study, the adsorption cross sections for complexes **6–8** and the N3 dye were determined by dipping the TiO<sub>2</sub> film into each dye solution. After soaking for more than 16 h for complete adsorption, unbound dye molecules on TiO<sub>2</sub> films were washed off by absolute ethanol. Then the bound dye molecules were desorbed by dipping into an ethanol solution of NaOH, and the number of dye molecules remaining in the basic solution was determined by UV-vis absorbance. It should be noticed that TiO<sub>2</sub> films were made by the same protocol as above and the roughness factors of the films, determined by Brunauer–Emmett–Teller (BET) experiments, were ca. 800. The molecular cross-sectional areas were calculated directly from the molecular radii, which were obtained by the Hartree-Fock method. The adsorption cross section was then derived by the ratio of the number of dye versus the real surface area of the TiO<sub>2</sub> film. The latter was deduced by the multiplication of the geometric area of the TiO<sub>2</sub> film and the roughness factor.

### 5.6. Theoretical Approaches

All calculations were performed with the Gaussian 03 package [25]. Geometrical optimization of the electronic ground state was carried out by the hybridized DFT functional, PBE0 and the basis set 6–31G\* was used for all atoms except for the Ru atom [26]. For Ru, the “double- $\zeta$ ” quality basis set consisted of the effective core potential SBKJC [27]. Time-dependent DFT (TDDFT) calculations were then performed with the same functional and basis set at the optimized geometry to obtain electronic transition energies. Oscillator strengths were deduced from the dipole transition matrix elements (for singlet states only). The Hartree-Fock method with the same basis set was applied to

calculate the molecular volume, which is defined as the electron density inside a contour of 0.001 electrons/bohr<sup>3</sup>. Furthermore, as recommended by the Gaussian 03 package, the radius was selected to be 0.5 Å larger than that deduced from the computed volume.

Received: October 20, 2006

Revised: February 21, 2007

Published online: August 28, 2007

- [1] M. K. Nazeeruddin, M. Grätzel, in *Molecular and Supramolecular Photochemistry* (Eds: V. Ramamurthy, K. Schanze), Vol. 10, Marcel Dekker, New York, NJ **2002**, pp. 301–343.
- [2] a) M. K. Nazeeruddin, A. Kay, I. Rodicio, R. Humphry-Baker, E. Muller, P. Liska, N. Vlachopoulos, M. Grätzel, *J. Am. Chem. Soc.* **1993**, *115*, 6382. b) M. K. Nazeeruddin, P. Pechy, T. Renouard, S. M. Zakeeruddin, R. Humphry-Baker, P. Comte, P. Liska, L. Cevey, E. Costa, V. Shklover, L. Spiccia, G. B. Deacon, C. A. Bignozzi, M. Grätzel, *J. Am. Chem. Soc.* **2001**, *123*, 1613. c) O. Kohle, S. Ruile, M. Grätzel, *Inorg. Chem.* **1996**, *35*, 4779.
- [3] a) M. Yanagida, T. Yamaguchi, M. Kurashige, K. Hara, R. Katoh, H. Sugihara, H. Arakawa, *Inorg. Chem.* **2003**, *42*, 7921. b) G. Sauve, M. E. Cass, S. J. Doig, I. Lauerma, K. Pomykal, N. S. Lewis, *J. Phys. Chem. B* **2000**, *104*, 3488. c) R. Argazzi, C. A. Bignozzi, T. A. Heimer, F. N. Castellano, G. J. Meyer, *Inorg. Chem.* **1994**, *33*, 5741. d) T. A. Heimer, E. J. Heilweil, C. A. Bignozzi, G. J. Meyer, *J. Phys. Chem. A* **2000**, *104*, 4256. e) A. S. Polo, M. K. Itokazu, N. Y. Mä Iha, *Coord. Chem. Rev.* **2004**, *248*, 1343–1361. f) N. Robertson, *Angew. Chem. Int. Ed.* **2006**, *45*, 2338. g) A. Islam, F. A. Chowdhury, Y. Chiba, R. Komiya, N. Fuke, N. Ikeda, K. Nozaki, L. Han, *Chem. Mater.* **2006**, *18*, 5178. h) C.-Y. Chen, S.-J. Wu, C.-G. Wu, J.-G. Chen, K.-C. Ho, *Angew. Chem. Int. Ed.* **2006**, *45*, 5822.
- [4] a) C.-C. Cheng, W.-S. Yu, P.-T. Chou, S.-M. Peng, G.-H. Lee, P.-C. Wu, Y.-H. Song, Y. Chi, *Chem. Commun.* **2003**, 2628. b) P.-T. Chou, Y. Chi, *Eur. J. Inorg. Chem.* **2006**, 3319. c) P.-T. Chou, Y. Chi, *Chem. Eur. J.* **2007**, *13*, 380.
- [5] A. Islam, H. Sugihara, M. Yanagida, K. Hara, G. Fujihashi, Y. Tachibana, R. Katoh, S. Murataa, H. Arakawa, *New J. Chem.* **2002**, *26*, 966.
- [6] a) K.-J. Jiang, N. Masaki, J.-B. Xia, S. Noda, S. Yanagida, *Chem. Commun.* **2006**, 2460. b) S.-R. Jang, R. Vittal, J. Lee, N. Jeong, K.-J. Kim, *Chem. Commun.* **2006**, 103. c) D. P. Hagberg, T. Edvinsson, T. Marinado, G. Boschloo, A. Hagfeldt, L. Sun, *Chem. Commun.* **2006**, 2245.
- [7] A. Hagfeldt, M. Grätzel, *Acc. Chem. Res.* **2000**, *33*, 269.
- [8] a) E. C. Constable, F. Heitzler, M. Neuburger, M. Zehnder, *J. Am. Chem. Soc.* **1997**, *119*, 5606. b) K. Chen, Y.-M. Cheng, Y. Chi, M.-L. Ho, C.-H. Lai, P.-T. Chou, S.-M. Peng, G.-H. Lee, *Chem. Asian J.* **2007**, *2*, 155.
- [9] T. Kaminski, P. Gros, Y. Fort, *Eur. J. Org. Chem.* **2003**, 3855.
- [10] a) A. R. Oki, R. J. Morgan, *Synth. Commun.* **1995**, *25*, 4093. b) M. K. Nazeeruddin, P. Pechy, T. Renouard, S. M. Zakeeruddin, R. Humphry-Baker, P. Comte, P. Liska, L. Cevey, E. Costa, V. Shklover, L. Spiccia, G. B. Deacon, C. A. Bignozzi, M. Grätzel, *J. Am. Chem. Soc.* **2001**, *123*, 1613.
- [11] D. P. Rillema, D. S. Jones, C. Woods, H. A. Levy, *Inorg. Chem.* **1992**, *31*, 2935.
- [12] M. Abrahamsson, H. Wolpher, O. Johansson, J. Larsson, M. Kritikos, L. Eriksson, P.-O. Norrby, J. Bergquist, L. Sun, B. Åkermark, L. Hammarström, *Inorg. Chem.* **2005**, *44*, 3215.
- [13] Y.-L. Tung, S.-W. Lee, Y. Chi, L.-S. Chen, C.-F. Shu, F.-I. Wu, A. J. Carty, P.-T. Chou, S.-M. Peng, G.-H. Lee, *Adv. Mater.* **2005**, *17*, 1059.
- [14] Y.-L. Tung, L.-S. Chen, Y. Chi, P.-T. Chou, Y.-M. Cheng, E. Y. Li, G.-H. Lee, C.-F. Shu, F.-I. Wu, A. J. Carty, *Adv. Funct. Mater.* **2006**, *16*, 1615.
- [15] a) M. L. Scudder, D. C. Craig, H. A. Goodwin, *Cryst. Eng. Commun.* **2005**, *7*, 642. b) S. Pyo, E. Perez-Cordero, S. G. Bott, L. Echegoyen, *Inorg. Chem.* **1999**, *38*, 3337.

- [16] M. K. Nazeeruddin, S. M. Zakeeruddin, J.-J. Lagref, P. Liska, P. Comte, C. Barolo, G. Viscardi, K. Schenk, M. Grätzel, *Coord. Chem. Rev.* **2004**, *248*, 1317.
- [17] S. M. Zakeeruddin, M. K. Nazeeruddin, P. Pechy, F. P. Rotzinger, R. Humphry-Baker, K. Kalyanasundaram, M. Grätzel, V. Shklover, T. Haibach, *Inorg. Chem.* **1997**, *36*, 5937.
- [18] R. H. Herber, G. Nan, J. A. Potenza, H. J. Schugar, A. Bino, *Inorg. Chem.* **1989**, *28*, 938.
- [19] C. C. Cheng, J. G. Goll, G. A. Neyhart, T. W. Welch, P. Singh, H. H. Thorp, *J. Am. Chem. Soc.* **1995**, *117*, 2970.
- [20] M. K. Nazeeruddin, Q. Wang, L. Cevey, V. Aranyos, P. Liska, E. Figemeier, C. Klein, N. Hirata, S. Koops, S. A. Haque, J. R. Durrant, A. Hagfeldt, A. B. P. Lever, M. Grätzel, *Inorg. Chem.* **2006**, *45*, 787.
- [21] a) A. V. Titov, N. S. Mosyagin, V. F. Ezhov, *Phys. Rev. Lett.* **1996**, *77*, 5346. b) W. C. Ermler, M. M. Marino, *J. Chem. Inf. Comput. Sci.* **2001**, *41*, 77. c) A. V. Titov, N. S. Mosyagin, *Int. J. Quant. Chem.* **1999**, *71*, 359. d) A. V. Titov, *Int. J. Quant. Chem.* **1998**, *57*, 453.
- [22] a) E. Duliere, M. Devillers, J. Marchand-Brynaert, *Organometallics* **2003**, *22*, 804. b) M. A. Bennett, T. N. Huang, T. W. Matheson, A. K. Smith, *Inorg. Synth.* **1982**, *21*, 74.
- [23] N. Papageorgiou, W. F. Maier, M. Grätzel, *J. Electrochem. Soc.* **1997**, *144*, 876.
- [24] C. Klein, M. K. Nazeeruddin, D. Di Censo, P. Liska, M. Grätzel, *Inorg. Chem.* **2004**, *43*, 4216.
- [25] M. J. Frisch, G. W. Trucks, H. B. Schlegel, G. E. Scuseria, M. A. Robb, J. R. Cheeseman, Jr., J. A. Montgomery, T. Vreven, K. N. Kudin, J. C. Burant, J. M. Millam, S. S. Iyengar, J. Tomasi, V. Barone, B. Mennucci, M. Cossi, G. Scalmani, N. Rega, G. A. Petersson, H. Nakatsuji, M. Hada, M. Ehara, K. Toyota, R. Fukuda, J. Hasegawa, M. Ishida, T. Nakajima, Y. Honda, O. Kitao, H. Nakai, M. Klene, X. Li, J. E. Knox, H. P. Hratchian, J. B. Cross, V. Bakken, C. Adamo, J. Jaramillo, R. Gomperts, R. E. Stratmann, O. Yazyev, A. J. Austin, R. Cammi, C. Pomelli, J. W. Ochterski, P. Y. Ayala, K. Morokuma, G. A. Voth, P. Salvador, J. J. Dannenberg, V. G. Zakrzewski, S. Dapprich, A. D. Daniels, M. C. Strain, O. Farkas, D. K. Malick, A. D. Rabuck, K. Raghavachari, J. B. Foresman, J. V. Ortiz, Q. Cui, A. G. Baboul, S. Clifford, J. Cioslowski, B. B. Stefanov, G. Liu, A. Liashenko, P. Piskorz, I. Komaromi, R. L. Martin, D. J. Fox, T. Keith, M. A. Al-Laham, C. Y. Peng, A. Nanayakkara, M. Challacombe, P. M. W. Gill, B. Johnson, W. Chen, M. W. Wong, C. Gonzalez, J. A. Pople, *Gaussian 03*, Gaussian Inc., Wallingford, CT **2004**, Revision C.02.
- [26] C. Alamo, G. E. Scuseria, V. Barone, *J. Chem. Phys.* **1999**, *111*, 2889.
- [27] W. J. Stevens, M. Krauss, H. Basch, P. G. Jasien, *Can. J. Chem.* **1992**, *70*, 612.